Rodriguez-Sanchez, M. R., Santana, D. & Olalde, G. (2016). Experimental study of honeycomb SiCSi under highly concentrated solar flux: Evolution of its thermo-radiative properties. *Solar Energy Materials and Solar Cells*, 155, pp. 253–263.

DOI: 10.1016/j.solmat.2016.06.032

Experimental study of honeycomb SiCSi under highly concentrated solar flux: evolution of its thermo-radiative properties

M.R. Rodriguez-Sanchez[1*], D. Santana[1], G. Olalde[2].

[1] Energy Systems Engineering Group (ISE), Department of Fluids and Thermal Engineering, Universidad Carlos III of Madrid.

Av. Universidad 30, Leganés, 28911, Madrid, Spain

[2] Laboratoire PROcédés, Matériaux, Energie Solaire (PROMES), UPR 8521 CNRS.

7 rue du Four Solaire, 66120 Odeillo, France.

*Phone number: +34 916246034, Fax: +34916249430, e-mail: mrrsanch@ing.uc3m.es

Abstract

The material that is used in solar receivers is subjected to intense cyclic thermal stresses and extreme temperatures, which are directly dependent on the intermittence of the solar resource. These factors accelerate the ageing mechanisms and reduce the durability of the receivers because of a reduction of their thermal performance.

This study presents guidelines to study the thermo-radiative properties of an absorber material that is subjected to a highly concentrated solar flux. The material was a square honeycomb SiCSi structure that is typically used in volumetric air receivers. Accelerated ageing tests were performed by means of crashing thermal treatments, in which the modulus and period of the incident flux and the boundary conditions of the material were varied.

The reflectivity and absorptivity of the material were experimentally characterized before and after the thermal treatments. The measurements were performed using two different reflectometers, one monochromatic and one in the solar band; the latter can measure at ambient temperature or high temperature that is representative of the operational conditions (400 - 700 ºC). However, only the solar band reflectometer working at high temperature was able to detect the evolution of the thermo-radiative properties of the material, which highlights the important role of the temperature and the wavelength. Furthermore, the thermal treatments in which the samples were water-cooled and in which the solar flux was medial more quickly accelerated the ageing mechanism of the material and reduced its absorptivity.

Keywords

Volumetric solar receiver; SiCSi; reflectivity; absorptivity; ageing; durability.

Nomenclature

Abbreviations

A : Samples in which the incident flux is intercepted by the sheet side.

B : Samples in which the incident flux is intercepted by the honeycomb face.

BC : Boundary conditions.

CSP: Concentrating solar power.

DISCO: Solar band reflectometer.

DNI: Direct normal irradiance.

nt: Non-treated or raw sample.

REFFO: Monochromatic optical fibre reflectometer.

SAAF: Accelerating age facility.

TT : Thermal treatment.

Symbols

E : Energy per unit surface area [W/m^2].

k : Conductivity [W/mK].

T : Temperature [K].

T_{amb} : Ambient temperature [K].

α : Absorptivity [-].

$\alpha_s^{\perp}$: Normal absorptivity [-].

ε : Emissivity [-].

ϕ_{air} : Absorbed solar flux [W/m^2].

ϕ_i : Incident solar flux [W/m^2].

η_{rec} : Receiver efficiency [-].

$\rho_s^{\perp\cap}$: Hemispherical reflectivity [-].

Subscripts

a : Adiabatic.

i : Isothermal.

s : Steady.

u : Un-steady.

1 : Incident solar flux 1000 KW/m^2.

2 : Incident solar flux 700 KW/m^2.

3 : Incident solar flux 500 KW/m^2.

1. Introduction

Concentrating Solar Power (CSP) is a promising source of clean energy in modern society. While solar energy offers the highest renewable energy potential to our planet, CSP can provide dispatchable power in a technically viable way by means of thermal energy storage and/or hybridization [1]. One of the main challenges of CSP is to reduce the levelized cost of electricity to improve its competitiveness with respect to conventional electricity generation. To achieve this goal, the durability of the materials is a crucial issue for designing reliable systems with high efficiencies and low maintenance costs [2]. Durability is defined as the capability of withstanding repeated use over a relatively long period of time to fulfil the design conditions.

Solar receivers are one of the main subsystems of CSP. They absorb the concentrated solar flux and transfer it to the heat transfer fluid with the greatest possible efficiency. Therefore, the receivers are exposed to highly concentrated solar fluxes, intense thermal stresses and high temperatures, which are known to be the major ageing factors of the materials [3]. From this perspective, specific materials have been developed to fulfil the requirements of solar receivers and maintain their performance over time. However, the early evolution of some of the critical properties of the materials, such the thermo-radiative properties (absorptivity,

emissivity) and thermo-physical properties (diffusivity, effusivity), causes the thermal efficiency of the receiver to deteriorate gradually to the failure limit, at which point the efficiency is not sufficient, and the receiver has to be replaced.

The most reliable way to assess the durability of the receiver's material is to test it under real operational conditions over long periods of time. However, this method is expensive and delays the development of technology. Therefore, the idea of performing thermal treatments (TTs) under extreme conditions, which accelerate the ageing of the receiver, has arisen. This method allows large numbers of extreme cycles to be performed over short periods of time, which aids in predicting the evolution of the properties of the materials and their durability.

Few studies have focused on the evolution of the thermo-radiative properties of the materials that are used in high-temperature solar receivers. Carlsson et al. [4] studied the durability and methods to accelerate the ageing of materials that are used in low-temperature solar systems and developed a performance criterion for flat-plate receivers. Rojas-Morín and Fernández-Reche [5] studied the thermal fatigue lifetime of Inconel-625 exposed to high solar radiation. Boubault et al. [2] determined the optimal conditions to accelerate the ageing of a coated two-layer metal using a numerical thermal model that was validated with experimental tests. The results of the optimal tests were published two year later [3]. Capeillère et al. [6] simulated the thermo-mechanical behaviour of a ceramic plate solar receiver, and Fend et al. [7] experimentally determined the thermo-physical properties of porous materials that are used in volumetric receivers. However, the latter two studies were carried out on unexposed materials. Experimental studies of the durability of ceramic solar receivers, such as SiCSi, were not found in the literature.

Therefore, in this study, square honeycomb samples of SiCSi, which are typically used in air volumetric receivers, were thermally treated in a solar-accelerated ageing facility (SAAF) at the PROMES laboratory. The TTs consisted of constant irradiance cycles and periodic square variations of the irradiance, which led to an enhancement of the ageing mechanisms due to variations of the temperature and thermal gradients. To determine the degradation of the SiCSi samples, the normal absorptivity was estimated before and after the TTs and was compared. The normal absorptivity was calculated in three ways using two different devices: 1) a reflectometer of optical fibre (REFFO), 2) an optical fibre solar reflectometer (DISCO) at ambient temperature and 3) a DISCO at a high representative temperature. It was thus possible to determine the importance of the wavelength and temperature in measuring the

thermo-radiative properties of the materials. Moreover, the degradation of the material can be studied as a function of the different ageing factors that were tested during the TT.

2. Study material

Over the past few decades, numerous materials have been used in solar receivers. The first receivers were built with standard stainless steels, which resulted in high corrosion and degradation [8]. Hence, a generation of high nickel alloys emerged to solve these problems. However, these high nickel alloys cannot withstand temperatures over 800 ^{o}C, so they need to be coated to improve the receiver absorptivity. The most common coating, the black paint *Pyromark*, undergoes high degradation under highly concentrated solar fluxes [9]. Although advanced metals are currently being developed, they all have problems associated with coating degradation. Therefore, the new generation of solar receivers that will be used in Brayton cycles, which reach temperatures up to 1000 ^{o}C, must be built with other types of materials, such as ceramic materials.

Ceramic materials have been successfully used in volumetric air receiver applications, such as HiTRec-I, HiTRec-II, Solair-200 and Solair-3000. The main problem of volumetric air receivers is the flow instability. However, in 1996, DLR showed that SiCSi honeycomb absorbers had the best results in terms of the application temperature, thermal shock resistance, and flow stability, which guaranteed a high thermal efficiency of the receivers [10].

Silicon carbide is composed of 20% silica and 80% carbon. SiCSi is used for high performance ceramic devices such as heat-exchangers, seal-rings, valve-discs and ceramic engine parts [11]. Its large field of applications is due to its outstanding properties, including good resistance to oxidation and corrosion, excellent thermal conductivity and high mechanical strength up to 1300 ^{o}C. However, at temperatures above 1400 ^{o}C, the mechanical properties (e.g., strength and creep) deteriorate due to the existing free silicon content [12]. Furthermore, this ceramic has particular advantages in terms of production and costs because it can be produced at relatively low temperatures. SiCSi is widely used in solar receiver applications due to its properties, which allow using the unspoiled material without a coating. For open volumetric receivers, the SiCSi is typically designed like a honeycomb.

This study analysed a honeycomb SiCSi structure from the company SCHUNCK with an absorptivity of 0.9 [7]. This material is equivalent to those used in the demonstration receiver Solair-3000 (Figure 1). The main advantage of this honeycomb structure in an open volumetric

receiver is that it produces a stable 2D air flow. However, during the receiver operation, hot spots can form and damage the receiver.

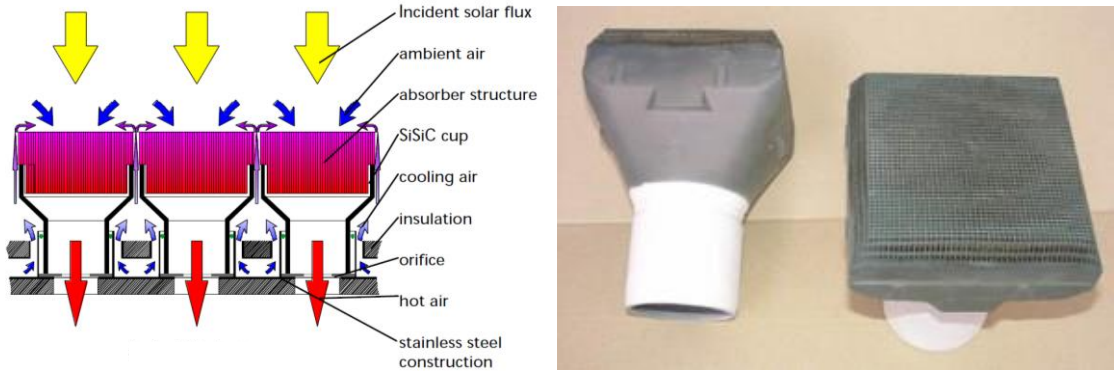

(a) (b)

Figure 1: a) Operational principles of Solair-3000 [13]. b) 140 mm × 40 mm units mounted in Solair-3000 [14].

The selected honeycomb SiCSi structure is composed of 2 mm x 2 mm square channels with the same depth as that of the absorber structure. The channels have a wall thickness of 0.8 mm. The honeycomb structure is non-symmetric in all directions. During normal operation of the receiver, the incident flux is parallel to the receiver channels; thus, the receiver channel direction is considered the main direction of the structure.

To carry out this study, the absorber structure was cut into two types of small samples using a diamond cutting system. Both types of samples are 15 mm x 15 mm square and 6 mm wide, and the solar flux during the TT was intercepted by one of the square faces. The type *A* samples were cut from the principal block in the secondary direction of the structure, so the face that intercepts the solar flux corresponds to a plane wall. The type *B* samples were cut in the main direction of the block, and the face that intercepts the solar radiation is composed of 5 x 5 channels that are 6 mm long (Figure 2). Therefore, the normal absorptivity of each type of sample is considerably different due to the geometric differences between the faces that intercept the solar irradiation.

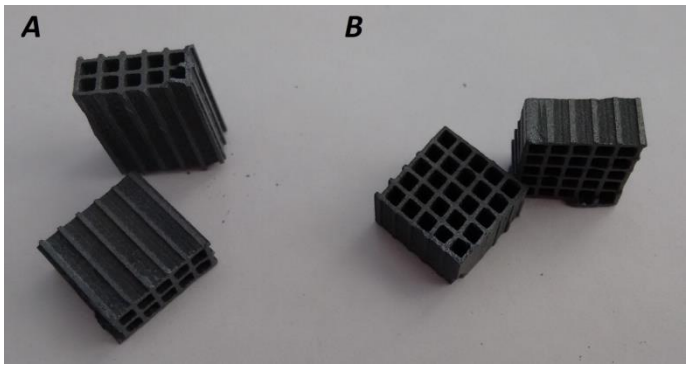

Figure 2. Type *A* and *B* SiCSi honeycomb samples.

It is important to note that the cutting of the samples is not very accurate, so the surfaces of the samples are non-homogeneous. Although the front surface of volumetric receivers is equivalent to the type *B* samples, that surface is difficult to characterize due to the irregularity that is caused by the numerous honeycomb cells. Therefore, type *A* samples are required to understand the evolution of the optical properties of SiCSi.

3. Thermal treatments

This section describes the experimental facility that was used to carry out the TTs and the selected TTs.

3.1. Experimental set-up: SAAF

The SAAF was developed at the CNRS-PROMES laboratory (Odeillo, France) to expose samples to controlled solar irradiances (Figure 3).

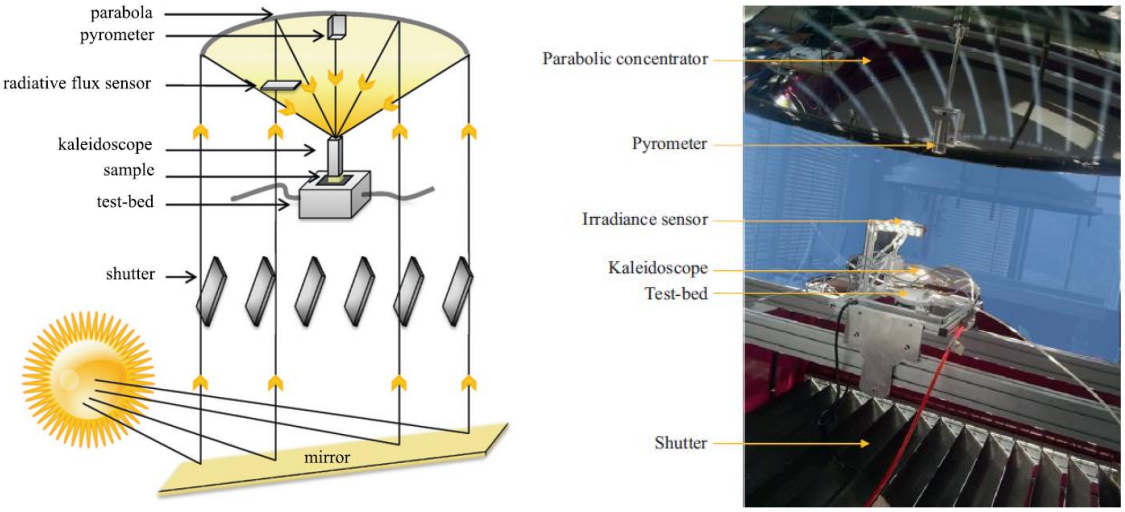

(a) (b)

Figure 3: a) Schematic of the Solar Accelerated Ageing Facility (SAAF) [15]. b) SAAF [3].

A 20-square-meter heliostat reflects solar rays towards a 2-meter-diameter parabolic concentrator that is capable of concentrating the light by 16,000 times. Thirteen rotary blade-shutters allow the amount of incident solar power to be controlled precisely via an irradiance sensor coupled with a PID regulation loop. The concentrated solar flux is homogenized using a water-cooled 20 mm x 20 mm x 60 mm mirror kaleidoscope before hitting the surface of the samples [3].

The sample is located at the focal point of the parabolic concentrator and is held in a metallic (AU4G) water-cooling test bed, which is able to withstand high temperatures (Figure 4). The sample is placed on a 50 mm x 50 mm copper sheet, which could be cooled by water.

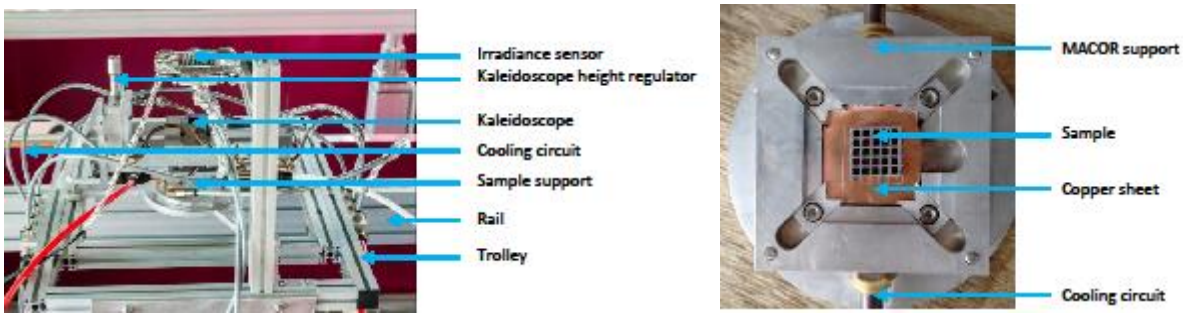

(a) (b)

Figure 4: a) SAAF trolley zoom. b) MACOR support.

An infrared solar-blind pyrometer was installed above the sample to monitor the surface temperature by collecting the flux emitted by the sample at a wavelength of 5.2 µm. The diameter of the optical target was 7.45 mm, which is the same order of magnitude as the wall thickness of the sample; this caused reliability problems for the temperature measurements of the type *B* samples. In these samples, the target section encompassed the front wall of the honeycomb, the cavity of the honeycomb, and the copper sheet.

3.2. Selection of thermal treatments

This study is motivated by the deterioration of the thermal performance of the receivers as a result of the alteration of the material due to ageing [3]. The thermal performance of the receiver is defined by the ratio of the energy that is absorbed by the heat transfer fluid to the incident flux on the receiver (Equation 1).

$$\eta_{rec} = \frac{\phi_{air}}{\phi_i} \qquad \text{(Equation 1)}$$

A thermal treatment strategy was designed taking into account the factors that most affect the ageing of the material. Boubault et al. and Lalau et al. [2,16] determined that the total exposure time, the flux intensity, and the boundary conditions of the samples (BCs) are the main ageing mechanisms for metallic and ceramic plates. They also highlighted the importance of studying the effects of steady and cyclic irradiation separately because they have different effects on the temperature and the thermal gradients. Figure 5 depicts the procedure that was used to study the ageing evolution of a solar receiver.

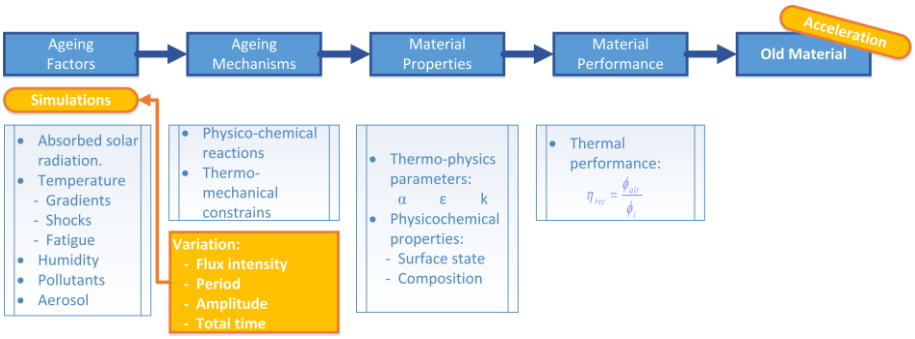

Figure 5. Accelerated ageing scheme [16].

This study is mainly focused on experimentally accelerating the age of honeycomb SiCSi samples in the SAAF using the most aggressive TTs given by [2,16]. This experimental study is not capable of following the evolution of the receiver performance. However, it can predict the evolution of the thermo-radiative properties and particularly the normal absorptivity of the honeycomb raw material.

Lalau et al. [16] selected fifteen TTs for a previous analysis of SiC and found that the period of the cyclic TT was not a significant factor in the ageing of the material. Thus, in this study, the number of TTs could be reduced to 7, including cyclic and steady TTs. All of the TTs were as long as possible (3 hours), and the solar flux varied from 500 kW/m^2 to 1000 kW/m^2. The cyclic TTs used periods of 60 seconds with square-shaped irradiance cycles (Figure 6b). Note that square cycles have higher energy for a fixed amplitude and period than other cycle shapes, which allows higher stress factors to be obtained [2].

During the TTs in the SAAF, the front surface and the side of the samples were in direct contact with the external ambient air and were subjected to natural convection. In contrast, isothermal or adiabatic BCs were used on the rear surface. The first BC was achieved by means of a water flow at 10 ^{o}C that cooled the rear face of the copper sheet to maintain a constant temperature at the contact between the copper sheet and the sample. The cooling water was

not used for the adiabatic BC, and a fibreglass layer was placed between the sample and the copper sheet.

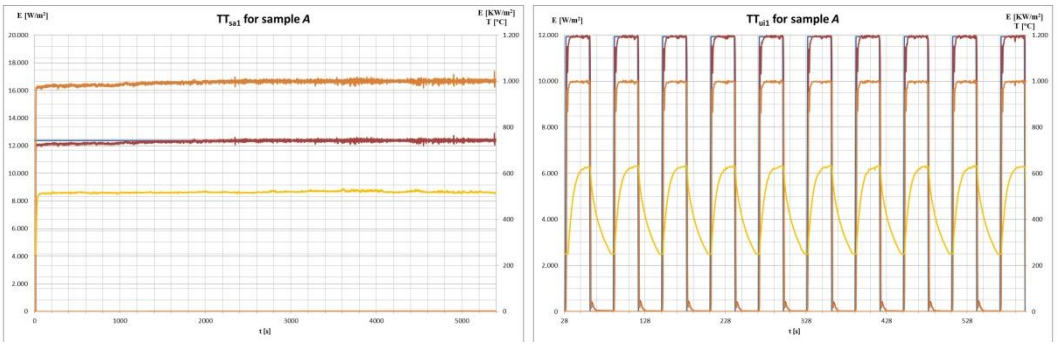

(a) (b)

Figure 6. a) Example of a steady state TT at 1000 kW/m^2. b) Example of an un-steady state TT at 1000 kW/m^2. The blue line corresponds to the constant value on the PID (left axis), the red line corresponds to the solar flux that is intercepted by the irradiance sensor (left axis), the yellow line corresponds to the surface temperature that is measured with the pyrometer (right axis), and the orange line is the solar flux on the sample (right axis).

Table 1 summarizes the seven TTs that were used on the samples in this study. A total of eight samples were used for each type of sample: seven for the different TTs (treated samples) and one raw (non-treated) sample.

Table 1: Summary of the TTs applied to both types of samples. Yellow indicates the TTs in which the samples were cooled by water (isothermal BC), and red indicates the TTs in which the samples were isolated (adiabatic BC). Subscripts: u: un-steady; s: steady; i: isothermal; a: adiabatic; 1: 1000 KW/m^2; 2: 700 KW/m^2; and 3: 500 KW/m^2.

Exposure time		3 hours	
Amplitude		**Un-steady state**	**Steady state**
Period [s]		60	-
Incident Flux [kW/m^2]	1000	**TT$_{ui1}$** **TT$_{ua1}$**	**TT$_{si1}$** **TT$_{sa1}$**
	700	**TT$_{ui2}$**	
	500	**TT$_{ui3}$**	**TT$_{sa3}$**

Table 2 shows the maximum temperature that was reached during the different TTs for sample types *A* and *B*. During the TT, the type *A* samples reached higher temperatures than the type *B* samples; thus, the usage of honeycomb structures reduces the wall temperature compared to the plane walls. Furthermore, the adiabatic BCs are more aggressive than the isothermal BCs.

Note also that TT_{ui2} had an unexpected low temperature for sample type *A* and an extremely high temperature for sample type *B*. TT_{sa3} for sample type A also resulted in a higher temperature than was expected.

Table 2: Summary of the maximum front surface temperatures reached during the different TTs that were applied to both types of samples. Yellow indicates the TTs with isothermal BCs, and red indicates adiabatic BCs.

Sample type	*A*		*B*	
Exposure time	3 hours		3 hours	
Amplitude	**Un-steady state**	**Steady state**	**Un-steady state**	**Steady state**
Period [s]	60	-	60	-
Maximum surface temperature [^{o}C]	**700 1050**	**375 525**	**450 700**	**325 525**
	275		**1000**	
	550	**800**	**400**	**475**

After carrying out the TTs, most of the samples had no visible changes (macroscopic level), which confirms the correct heat transfer fluid circulation in solar receiver applications. However, it should be noted that the type *A* sample that was thermally treated with TT_{ua1} was broken and that the type *B* samples that were thermally treated with TT_{sa3} and TT_{sa1} formed a series of bubbles at the surface that intercepted the solar flux (Figure 7). These exceptions verify that the adiabatic BCs are the most severe for both types of samples.

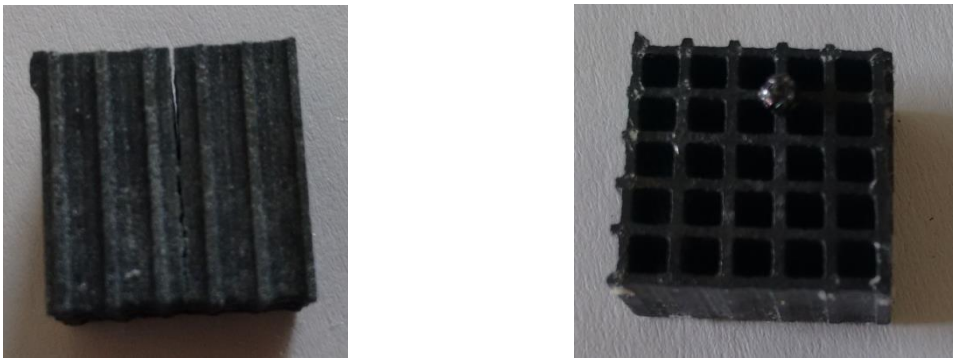

(a) (b)

Figure 7. a) Sample *A* after TT_{ua1}. b) Sample *B* after TT_{sa1}.

4. Normal absorptivity determination

The normal absorptivity of the material cannot be measured directly; thus, it is estimated from the directional normal solar reflectivity distribution. Two different reflectometers were used to characterize the thermo-radiative properties of both types of honeycomb SiCSi samples; a monochromatic reflectometer with a length of 0.83 µm (REFFO) was used at ambient

temperature, and a solar band reflectometer (DISCO) was used at ambient temperature and a representative high temperature.

By integrating the directional normal solar reflectivity distribution that was obtained with the reflectometers over the entire hemisphere, it is possible to estimate the hemispherical normal reflectivity in the solar spectrum, $\rho_s^{\perp\cap}$. Therefore, the normal solar absorptivity, $\alpha_s^{\perp}$, can be calculated by integration using Equation 2 [17]:

$$\alpha_s^{\perp} = 1 - \rho_s^{\perp\cap} \qquad \text{(Equation 2)}$$

This study also focused on finding the correct way to characterize the thermo-radiative properties of solar materials, which depend on the wavelength and the temperature. Therefore, a test was performed to determine whether a monochromatic optical fibre reflectometer is able to characterize the evolution of the normal absorptivity of ceramic absorbers or whether a solar band reflectometer is required. Furthermore, the deterioration of the thermo-radiative properties after the TT at ambient temperature was checked to determine whether it is equal to that at high temperatures. Both reflectometers and the measurement processes are described in the following subsections.

4.1. Monochromatic optical fibre reflectometer (REFFO)

REFFO measures the normal hemispherical and monochromatic reflectivity of the samples in the infrared spectrum at a wavelength of 0.83 µm.

A silica optical fibre with a diameter of 1 mm emits a monochromatic beam perpendicular to the surface of the sample. The reflected flux is collected by a series of seven receiving optical fibres that are distributed every ten degrees from 0˚ to 60˚ (Figure 8).

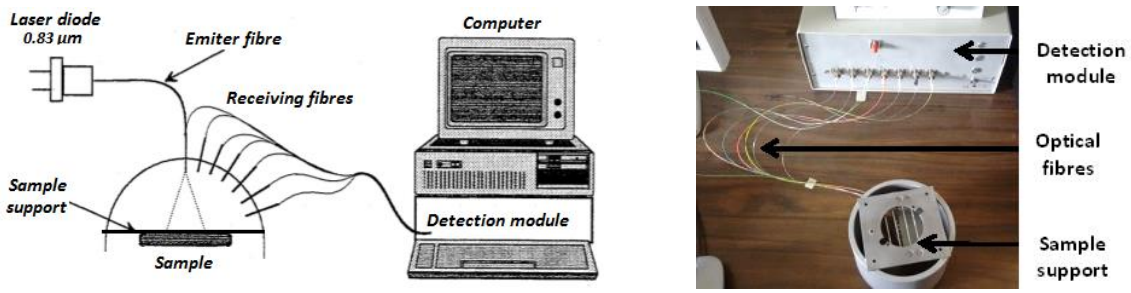

(a) (b)

Figure 8. a) Schematic of the REFFO device. b) REFFO device.

4.2. Solar band optical fibre reflectometer (DISCO)

A fibre reflectometer called DISCO was used to estimate the hemispherical reflectivity in the solar spectrum (visible wavelengths). The operational principles are similar to those of REFFO; an optical fibre emits a solar beam perpendicular to the surface of the sample, and eight fibres collect the reflected flux in different directions from 0˚ to 70˚ [18]. The solar beam that is emitted by DISCO is injected into the optical fibre by a convergent lens that receives the solar flux from a 3 m x 3 m square heliostat that is located adjacent to the device.

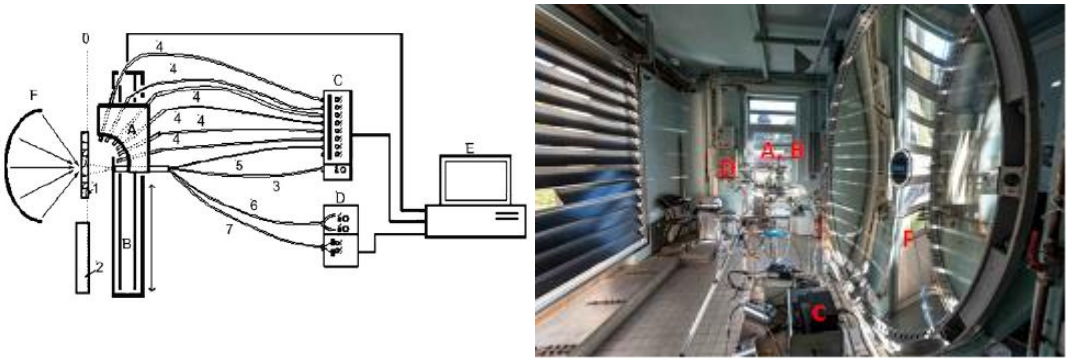

(a) (b)

Figure 9. a) Schematic of the DISCO device. A: Fibre basis cooled by water. B: Motorized trolley. C: Detection body. D: Pyroreflectometer. E: Computer. F: Parabola. 1: Sample, 2: Sphere lab. 3: Emission fibre. 4: Receiver fibres from 10˚ to 70˚. 5: Normal receiver fibre. 6: Laser Pyroreflectometer. 7: Pyroreflectometer receiver fibre. b) DISCO device.

DISCO can measure the reflectivity of the samples at different temperatures because the sample is placed at the focus of a 2-m-diameter parabola (Figure 9). A shutter system is used to control the solar irradiation that is intercepted by the sample. If the shutters are opened, the rear part of the sample is heated, and the reflectivity is measured by the non-irradiated face. The pyrometer that was previously used in the SAAF facility was employed to measure the temperature of the sample; it faced the non-irradiated surface of the sample. When the shutters were closed, the solar irradiation to be injected into the optical fibre passed through a hole in the middle of the shutters, but the sample remained at the ambient temperature.

5. Results and discussion

In this section, the normal absorptivity of both types of honeycomb SiCSi samples was characterized. In particular, the most influential parameters on the evolution of the normal

absorptivity were identified. The normal absorptivities of the treated and the non-treated samples were then characterized with the different devices and compared.

5.1. Characterization of raw samples (non-treated)

The honeycomb SiCSi samples *A* and *B* were characterized before performing the TTs. To reduce the error, the reflectivity measurements were repeated several times. In REFFO, they were repeated 25 times. However, due to the instability of the sun and the need for clear skies, only 7 repetitions were used to measure the reflectivity in DISCO.

Using REFFO, the average hemispherical reflectivities were 0.0895 for sample *A* and 0.0656 for sample *B* with standard deviations of 0.23% and 0.085%, respectively. At ambient temperature (10 - 15 ˚C), DISCO measured a hemispherical reflectivity of 0.0991 with a standard deviation of 0.62% for sample *A* and a hemispherical reflectivity of 0.0496 with a standard deviation of 0.58% for sample *B*. The higher standard deviation in sample *A* can be explained by a greater variation of the Direct Normal Irradiance (DNI) during the reflectivity tests of sample *A*.

At high temperatures, the shutters were opened, but maintaining a constant temperature was difficult because they were manually controlled. Therefore, a range of temperatures between 400 and 700 ˚C that were obtained during the TTs was allowed. The DNI during the test was approximately 100 W/m^2, and the shutters were never opened more than 20%. The shutters were opened for short periods of time to avoid overheating the samples and the fibres because they were not cooled.

Performing the measurements at high temperatures increased the dispersion of the results; the hemispherical reflectivity of the non-treated sample *A* was 0.0942, and the standard deviation 0.79%. The facility could not accurately measure sample *B* and obtained only one valid value for the hemispherical reflectivity (0.00818).

Table 3 summarizes the normal absorptivities of the non-treated samples *A* and *B*. The shape of the front face of the type *B* samples makes it similar to a black body, so the absorptivity of these samples is higher than that of the type *A* samples, whose surface is similar to a sheet.

The normal absorptivities that were obtained with the three types of measurements for the type *A* samples were very similar; they were approximately 1% higher when REFFO was used and slightly lower at ambient temperature than at high temperatures. Therefore, both devices can be used to characterize the material before the TTs. However, the normal absorptivities that were calculated for the type *B* samples by the different methods differed significantly by

approximately 4%. The difference was mainly associated with the focus point at which the reflectivity tests were performed.

DISCO at ambient temperature showed that sample *B* reflects very low energy, which indicates that no rays were reflected back to the receiving fibres in any direction, and the focus point was the inner part of a channel. However, the directional reflectivity of DISCO at high temperatures for sample *B* had a similar pattern to that for sample *A*; the reflectivity was measured at a focus point that was formed by the walls. Because the absorptivity that was measured with REFFO is between the other results, the fibres were measured at a focus point that was formed by walls and channels. These results demonstrate the difficulty of characterizing the type *B* samples.

Table 3. Normal absorptivity calculated using the REFFO and DISCO devices at different temperatures for the non-treated samples *A* and *B*.

Absorptivity	**REFFO**	**DISCO T_{amb}**	**DISCO T≈600 ^{o}C**
Sample *A*	0.91	0.901	0.906
Sample *B*	0.93	0.950	0.918

5.2. Characterization of treated samples

This subsection compares the normal absorptivity of the different samples after the TTs with the absorptivity of the non-treated samples. These comparisons were performed by varying only one parameter of the treatment, including the incident flux, the BC or the irradiation cycle. This subsection also focuses on the comparison between reflectometers.

Variation of the incident flux

Two series of TTs can be compared as a function of the incident flux. TT_{ui1}, TT_{ui2} and TT_{ui3} use periods of 60 seconds and isothermal conditions, and TT_{sa1} and TT_{sa3} use a constant flux and adiabatic conditions. The absorptivities of the SiCSi samples after these TTs are shown in Figure 10, in which the solid lines represent the average normal absorptivity for the non-treated type *A* and *B* samples using the different devices (colours), and the different symbols represent the average normal absorptivity for the five TTs described above that were measured with the different facilities (colours and shapes).

Consistent with Table 3, the results in Figure 10 show that the normal absorptivity for the three types of measurements varies less for the non-treated sample *A* than for sample *B*. Thus,

to understand the evolution of the normal absorptivity after the TTs, special attention will be paid to the behaviour of the type *A* samples.

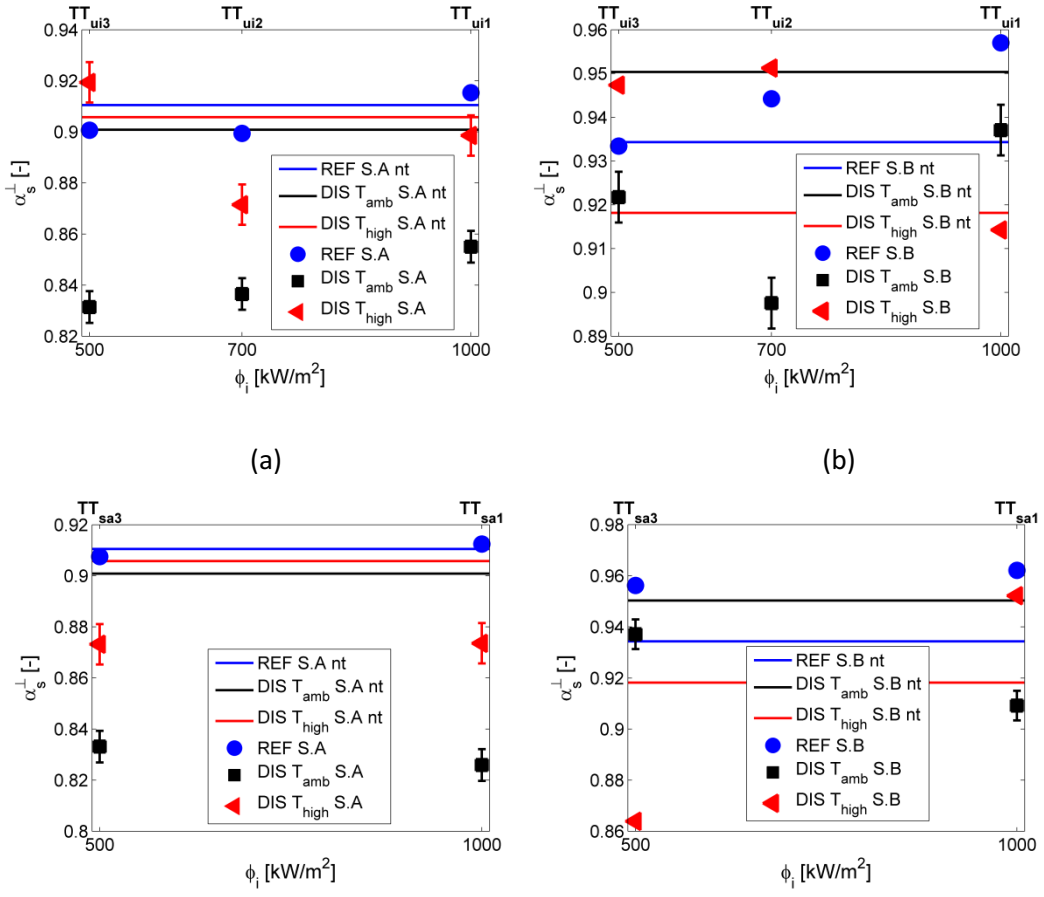

Figure 10. Effect of the incident flux on the normal absorptivity using a) 60 s period TT for type *A* samples, b) 60 s period TT for type *B* samples, c) steady state TT for type *A* samples, and d) steady state TT for type *B* samples.

Figure 10 also shows that the absorptivity that is measured with REFFO is nearly constant. The differences in the type *B* samples are due to the relative position of the focus point and the optical fibres. Thus, REFFO is not able to determine the ageing effect of the materials.

Using DISCO at ambient temperature, the absorptivity decreased after the TT and increased with the incident flux. The evolution of the absorptivity that was measured with DISCO at only high temperature can be observed in the type *A* samples. The flux of 500 kW/m^2 is not sufficient to accelerate the ageing of the SiCSi, and the absorptivity is the same as in the non-treated sample. At 700 kW/m^2, the degradation of the material is noticeable, and the absorptivity decreases; at 1000 kW/m^2, the temperature of the surface is so high that the absorptivity increases despite the material degradation and reaches similar values to that of

the non-treated sample. For all of the TTs, the normal absorptivities of the samples that were measured at high temperatures are higher than those at ambient temperature.

Variation of the irradiation cycle

By fixing the BC and the incident flux, a cyclic irradiance was studied to determine whether it more effectively activates the ageing mechanism of the SiCSi samples than a constant irradiance. Hence, two series of TTs were compared. TT_{ui1} and TT_{si1} used a flux of 1000 KW/m^2 and were cooled by water, and TT_{ua1} and TT_{sa1} used 1000 KW/m^2 and were isolated.

The results in Figure 11 confirm that REFFO cannot follow the absorptivity evolution of exposed SiCSi. Using DISCO, the absorptivity of the treated samples is lower than the absorptivity of the non-treated samples. Thus, both cyclic and steady treatments activate the ageing mechanisms of the SiCSi. The normal absorptivity is lower after constant irradiation than after cyclic irradiation because the deterioration of the material in the cyclic treatments is compensated for by the higher temperature. For sample *A*, the absorptivity of TT_{ua1} is lower than that of TT_{sa1} because the surface temperature in the first TT exceeded 1000 ^{o}C. At this temperature, the corrosion is severe, which accelerates the ageing mechanism of the SiCSi and reduces its absorptivity.

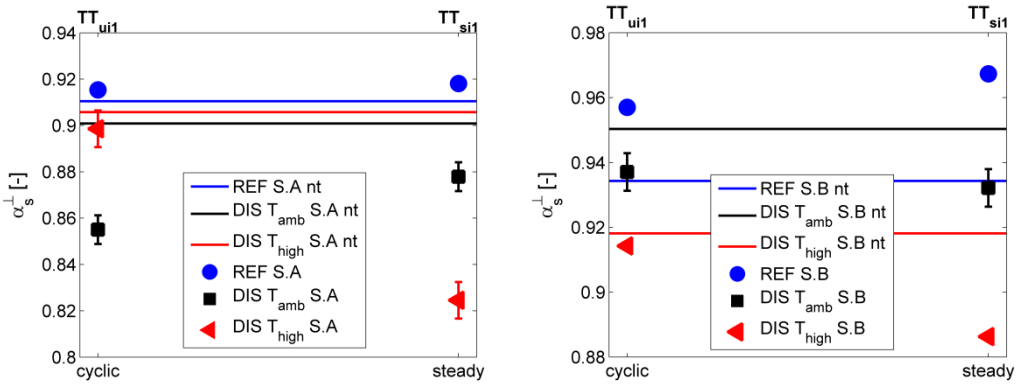

(a) (b)

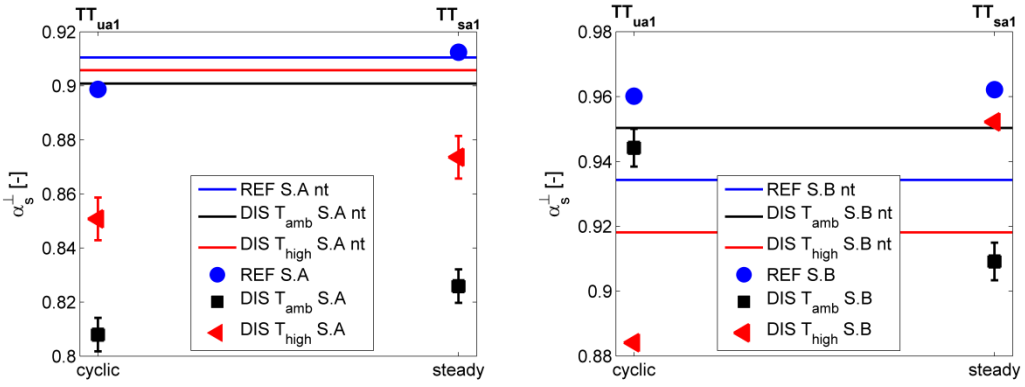

(c) (d)

Figure 11. Effects of the steady and unsteady TTs on the normal absorptivity when the samples are thermally treated with 1000 KW/m^2 and a) water-cooled for type *A* samples, b) water-cooled for type *B* samples, c) isolated for type *A* samples, and d) isolated for type *B* samples.

Variation of the boundary conditions

The effect of the BCs on the ageing mechanism of the SiCSi was studied using two series of thermal treatments; TT_{si1} and TT_{sa1} used a constant irradiance of 1000 kW/m^2, and TT_{ui1} and TT_{ua1} used a cyclic irradiance of 1000 kW/m^2. Figure 12 shows the absorptivities that were obtained for these samples.

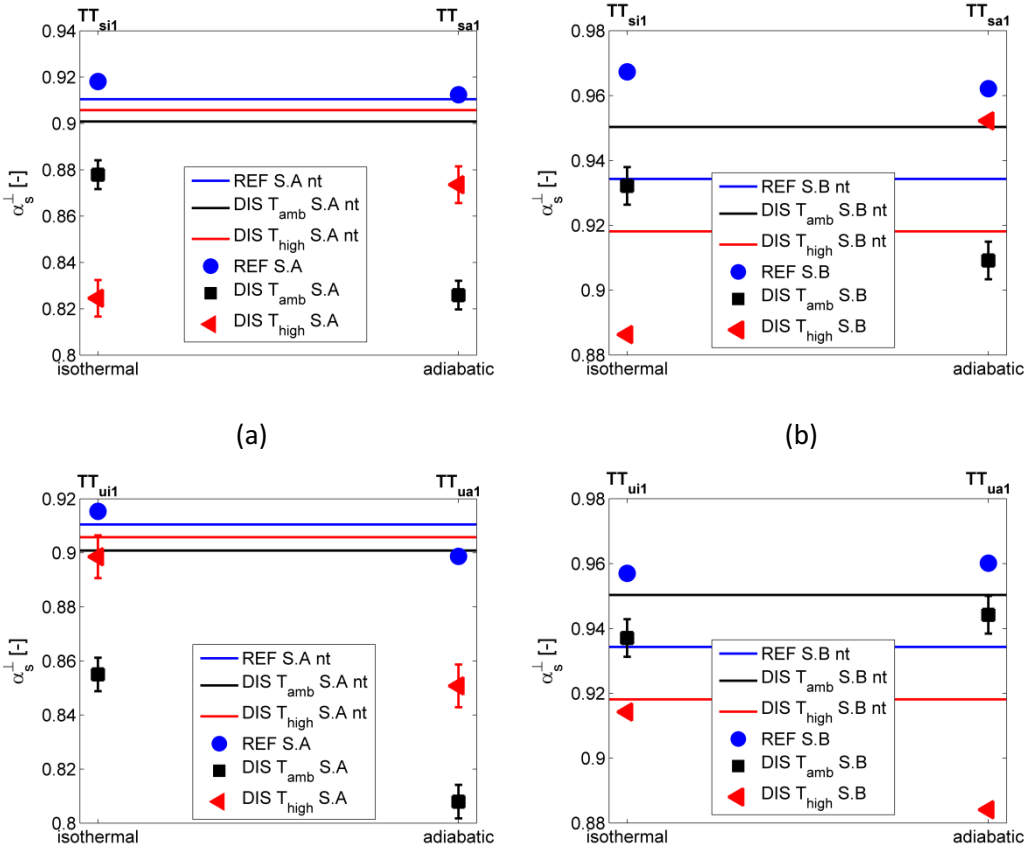

(a) (b)

(c) (d)

Figure 12. Effects of the isothermal and adiabatic BCs on the normal absorptivity for TTs of: a) 60 s period for type *A* samples, b) 60 s period for type *B* samples, c) steady state for type *A* samples, and d) steady state for type *B* samples.

Figure 12 shows that under the same operational conditions, the ageing mechanisms of the isolated and cooled samples depend on the surface temperature that is reached during the TT.

The cooled samples have lower absorptivities than the isolated samples unless than the temperature exceeds the corrosion limit.

6. Conclusions

In this study, the thermo-radiative properties of two types of SiCSi honeycomb samples were characterized before and after different TTs were carried out. These TTs are used to subject the samples to extreme operational conditions to accelerate their ageing mechanisms. All of the TTs were 3 hours long, and the incident solar flux, the irradiance shape and the BCs of the samples were varied.

During the TT, the type *A* samples received the concentrated solar flux perpendicular to the honeycomb, and the type *B* samples intercepted the solar flux in the same direction as the channels. Therefore, the type *A* samples do not correspond to a volumetric receiver, but they must be analysed. The reflectivity measurements depend on the focus point, and the type *B* samples are very heterogeneous, so it is difficult to characterize and follow the evolution of the optical properties of this type of samples.

The thermo-radiative properties of the honeycomb SiCSi were measured using two different devices: a monochromatic REFFO and a solar band DISCO. In the latter, two types of experiments were performed, including one at ambient temperature and one at high temperatures that are representative of the typical range of operation for solar receivers. The normal absorptivities that were obtained for the non-treated type *A* sample with the three tests were very similar. The dispersion for the type *B* sample was much greater due to the non-homogeneous surface.

The normal absorptivity of the samples decreases after any TT. However, the normal absorptivity is greater if high temperatures were reached during the TT than for the low temperature TT, and it could exceed the absorptivity of the non-treated samples. Thus, the factors that maximize the temperature tend to also increase the normal absorptivity. However, if the temperature of the surface exceeds 1000 ^{o}C, the material degrades drastically, and the absorptivity decreases abruptly. The lowest efficiency of the SiCSi was reached using the TT with intermediate concentrated solar fluxes, constant irradiance and the isothermal BC.

The results showed that the monochromatic REFFO could not detect the normal absorptivity variations before and after the TTs, which indicates that the wavelength that this device uses is not able to characterize the degradation of the optical properties of materials that are used in concentrating solar applications. The DISCO experiment showed the variations in the optical

properties before and after the TTs. In general, the tests that were performed at ambient and high temperatures have the same patterns, although the normal absorptivity at high temperatures is usually greater than that at ambient temperature.

Therefore, DISCO at ambient temperature can be used to determine the relative variation of the thermo-radiative properties of SiCSi due to exposure (aging effect). However, DISCO must be used at high temperatures to determine the absolute thermo-radiative properties of the samples. Nevertheless, DISCO at high temperatures gives a larger higher dispersion in the measurements and has some difficulty in performing the TTs, especially for the type *B* samples. Hence, a reference reflectivity should be measured at ambient temperature to demonstrate the coherence of the high temperature results.

Acknowledgements

The authors acknowledge the financial support of the research programme of the University Carlos III de Madrid, which made this study possible through a mobility grant. Moreover, this work was supported by the French "Investments for the future" programme, which is managed by the National Agency for Research under contract ANR-10-LABX-22-01, Labex SOLSTICE and by the Spanish government under the project ENE2012-34255.

References

[1] European energy research alliance, 2014. STAGE-STE project. http://www.stage-Ste.eu/. Accessed: 06/04/2016.

[2] A. Boubault, B. Claudet, O. Faugeroux, G. Olalde, J.J. Serra. A numerical thermal approach to study the accelerated aging of a solar absorber material. Sol. Energy. 86 (2012) 3153–3167.

[3] A. Boubault, B. Claudet, O. Faugeroux, G. Olalde. Aging of solar absorber materials under highly concentrated solar fluxes. Sol. Energy Mater. Sol. Cells. 123 (2014) 211–219.

[4] B. Carlsson, G. Jorgensen, M. Köhl. Performance and Durability Assessment. Elsevier, 2004.

[5] A. Rojas-Morín, J. Fernández-Reche. Estimate of thermal fatigue lifetime for the INCONEL 625-LCF plate while exposed to concentrated solar radiation. Rev. Metal. 47 (2011) 112–125.

[6] J. Capeillère, a. Toutant, G. Olalde, a. Boubault. Thermomechanical behavior of a plate ceramic solar receiver irradiated by concentrated sunlight. Sol. Energy. 110 (2014) 174–187.

[7] T. Fend, B. Hoffschmidt, R. Pitz-Paal, O. Reutter, P. Rietbrock. Porous materials as open volumetric solar receivers: Experimental determination of thermophysical and heat transfer properties. Energy. 29 (2004) 823–833.

[8] J.E. Pacheco. Final Test and Evaluation Results from the Solar Two Project. Albuquerque, SAND2002-0120, 2002.

[9] C.K. Ho, A. Roderick Mahoney, A. Ambrosini, M. Bencomo, A. Hall, T.N. Lambert. Characterization of Pyromark 2500 Paint for High-Temperature Solar Receivers. J. Sol. Energy Eng. 136 (2013) 4.

[10] B. Hoffschmidt, V. Fernandez, A.G. Konstandopoulos, I. Mavroidis, M. Romero, P. Stobbe, et al.. Development of ceramic volumetric receiver technology. 5th Col. Sol. Symp., Cologne (Germany), 2001: pp. 51–61.

[11] M. Wilhelm, S. Werdenich, W. Wruss. Influence of resin content and compaction pressure on the mechanical properties of SiC–Si composites with sub-micron SiC microstructures. J. Eur. Ceram. Soc. 21 (2001) 981–990.

[12] C.C. Agrafiotis, I. Mavroidis, A.G. Konstandopoulos, B. Hoffschmidt, P. Stobbe, M. Romero, et al.. Evaluation of porous silicon carbide monolithic honeycombs as volumetric receivers/collectors of concentrated solar radiation. Sol. Energy Mater. Sol. Cells. 91 (2007) 474–488.

[13] B. Hoffschmidt, F.M. Téllez, A. Valverde, J. Fernández, V. Fernández. Performance Evaluation of the 200-kWth HiTRec-II Open Volumetric Air Receiver. J. Sol. Energy Eng. 125 (2003) 87.

[14] P. Schild, 2003. Advanced solar volumetric air receiver for commercial solar tower power plants (SolAir). http://stobbe.com/research-Projects/solar-Energy/solair/. Accessed: 06/04/2016.

[15] A. Boubault, B. Claudet, O. Faugeroux, G. Olalde. Accelerated aging of a solar absorber material subjected to highly concentrated solar flux. Energy Procedia. 49 (2013) 1673–1681.

[16] R.Y. Lalau, T. Lebel, G. Olalde, O. Faugeroux, B. Claudet, R.G. Olalde. Étude expérimentale du vieillissement accéléré de matériaux pour récepteurs solaires et caractérisation des propriétés après traitement thermique. Odeillo, 2015.

[17] A. Boubault, B. Claudet, O. Faugeroux, N. Guerin, G. Olalde. Study of the aging of a solar ansorber material following thermoradiative and thermophysucal properties. High Temp. High Press. 42 (2013) 405–420.

[18] D. Hernandez, D. Antoine, G. Olalde, J.M. Gineste. Optical fiber reflectometer DISCO. J. Sol. Energy Eng. 121 (1999) 31–35.